

CAAP 2nd Annual Report

Date of Report: *September 30, 2020*

Contract Number: 693JK31850012CAAP

Prepared for: *USDOT Pipeline and Hazardous Materials Safety Administration (PHMSA)*

Project Title: *Magnet-assisted Fiber Optic Sensing for Internal and External Corrosion-induced Mass losses of Metal Pipelines under Operation Conditions*

Prepared by: *Missouri University of Science and Technology (Missouri S&T)*

Contact Information: *Genda Chen, Ph.D., P.E., Email: gchen@mst.edu, Phone: (573) 341-4462*

For quarterly period ending: *September 30, 2020*

Business and Activity Section

(a) General Commitments – Dr. Genda Chen directed the entire project and coordinated various project activities.

During the past reporting year, Mr. Ying Zhuo, Ph.D. candidate in civil engineering at Missouri S&T, was on board for this project. He is responsible for the fabrication and characterization test of sensors under Dr. Chen’s supervision. Drs. Chuanrui Guo and Liang Fan also contributed to this project.

(b) Status Update of Past Quarter Activities – Detailed updates are provided below by task.

Task 1 Optimization of a magnet-assisted hybrid FBG/EFPI sensor enclosed in a plexiglass container for simultaneous measurement of temperature and pipe wall thickness

Fig. 1 presents a schematic design of the proposed hybrid EFPI/FBG sensor for corrosion monitoring at one location of a pipeline. The sensor is composed of a gold-coated glass mirror and a lead-in fiber of the EFPI, a FBG sensor parallel to the EFPI, two glass tubes, a magnet, springs, and a protective enclosure. When the wall thickness of a pipe is reduced during corrosion, the magnetic force between the pipe and the magnet will be reduced, resulting in an increased spring displacement that will be measured by the increase in cavity length of the EFPI. Therefore, the change in cavity length represents the thickness of the pipe wall during corrosion tests. To ensure a stress-free condition when surrounded by soil in applications, each hybrid EFPI/FBG sensor is covered by a protective enclosure that is designed against soil pressure and attached on the external surface of a coated pipe with adhesives as illustrated in Fig. 1(a). A series of the sensors can be multiplexed to provide quasi-distributed monitoring of corrosion along the length of the pipeline as illustrated in Fig. 1(b).

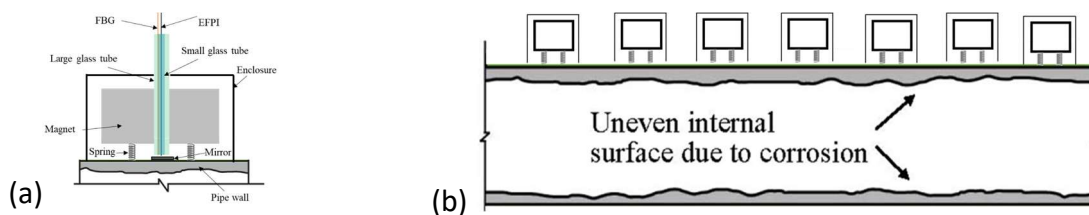


Fig. 1. (a) Schematic design of the proposed hybrid sensing system, and (b) quasi-distributed multiplexing fiber optic sensors in a pipeline application.

The hybrid EFPI/FBG sensor was manufactured in four steps as shown in Fig. 2. First, a gold-coated glass was glued to the top surface in center area of an 8 mm-thick steel plate, see Fig. 2(a). Second, 18 springs were uniformly distributed and glued to the surfaces of seven neodymium magnets that were placed inside a metal pan with a center hole, see Fig. 2(b). Third, a single mode fiber with an in-line FBG sensor was glued to the outside of a small-diameter glass tube that was fixed to a larger diameter glass tube. The bottom ends of the fiber and the two tubes were leveled, see Fig. 2(c). Fourth, the metal pan when turned upside down as shown in Fig. 2(d), was centered and placed on top of the steel plate. The large tube was inserted into the hole and fixed on the metal pan with a pre-determined distance from the steel plate. The hybrid sensor was completed after another single mode fiber cleaved at one end was passed through and glued to the small-diameter tube so that a desirable cavity length was achieved between the cleaved end of the lead-in fiber in an EFPI and the gold-coated glass mirror.

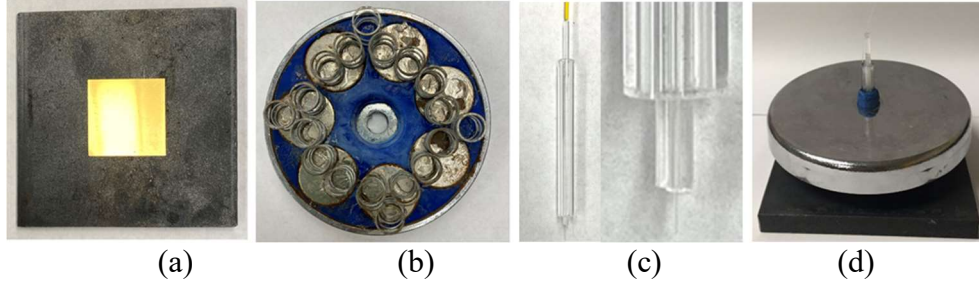


Fig. 2. (a) Gold-coated glass attached to the top surface of a steel plate, (b) springs glued to the surface of seven magnets in a metal pan, (c) assembling of a FBG sensor between two glass tubes, and (d) glass tubes glued to the metal pan with a single mode fiber passing through the inside tube.

Fig. 3 shows the accelerated corrosion test setup of a steel plate that supports the hybrid EFPI/FBG sensor. The steel plate in turn rested on a sponge that was halfway immersed in 3.5 wt.% Sodium Chloride (NaCl) solution in a plastic container. The four lateral sides of the steel plate were covered with marine epoxy to ensure no corrosion. Only the bottom surface of the steel plate was in contact with the solution and corroded. A copper wire was soldered on the top surface of the steel plate, and the solder spot was covered with marine epoxy for protection. During the corrosion test, the steel plate and a graphite rod were connected to the positive and negative electrodes of a DC power supply, respectively. A constant current ($1\text{mA}/\text{cm}^2$) was supplied to uniformly corrode the bottom surface of the steel plate, which was assumed to simulate the internal corrosion process of the pipeline. The signal from the EFPI sensor was measured every two hours at room temperature. The mass loss of the steel plate was calculated based on the Faraday's law:

$$\Delta m = WIt/nF \quad (1)$$

where W is the atomic weight of iron (56 g/mol); $I = A \cdot i$, $i = 1\text{mA}/\text{cm}^2$ and A is the cross section of the steel plate ($A = 6.25\text{ cm} \times 6.25\text{ cm}$); t is the time duration for impressing current to the steel plate; $n = 2$ ($\text{Fe} \rightarrow \text{Fe}^{2+}$); F is the Faraday constant (96,500 A s/mol). The thickness loss (τ) of the steel plate can be calculated based on Eq. (2):

$$\tau = \Delta m / \rho A \quad (2)$$

where ρ is the density of the steel plate ($7.85\text{ g}/\text{cm}^3$).

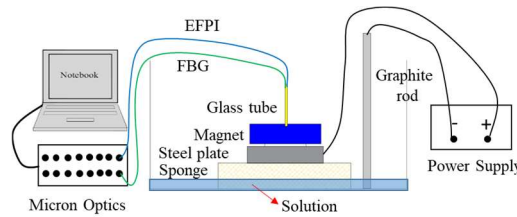


Fig. 3. Accelerated corrosion test of the steel plate with a magnet placed on its top through springs.

Fig. 4 shows the test results from a hybrid EFPI/FBG sensor with an initial cavity length of 730 μm . The cavity length of the EFPI decreases with the corrosion time or thickness loss of the steel plate. The test results were fitted with a polynomial function to the 3rd order, which can be used to predict the pipe wall thickness loss for the guidance of maintenance and rehabilitation.

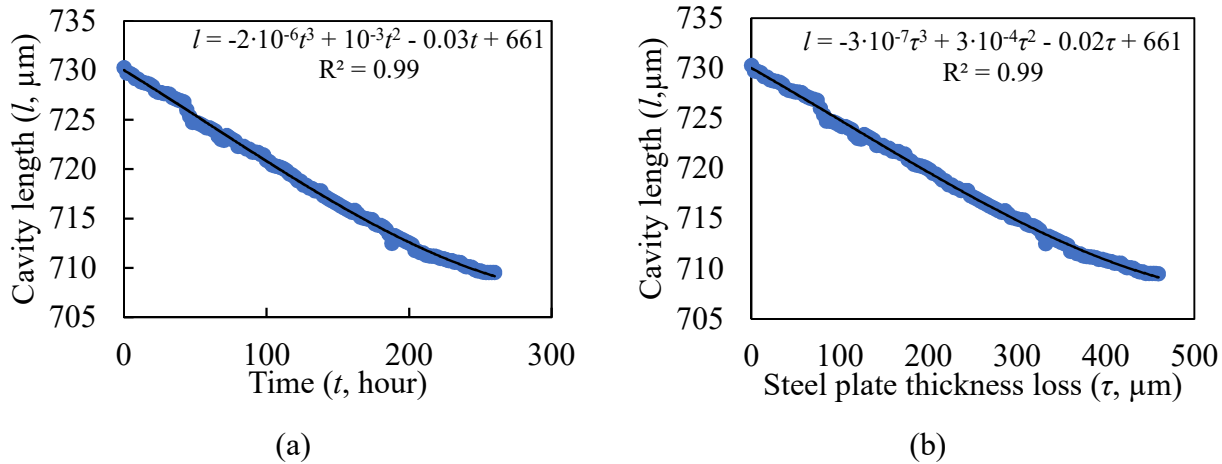


Fig. 4. Change of the cavity length of an EFPI sensor with: (a) the corrosion test time, and (b) thickness loss of the steel plate.

The temperature along a pipeline varies in different seasons. In addition, depending on the type of substances transported through the pipeline, the pipe may become locally warmer (crude oil, brine, heating systems) or cooler (gas pipeline). Therefore, the effect of temperature on the magnet-assisted hybrid EFPI/FBG sensor readings must be understood and compensated. In this study, the magnet-assisted hybrid EFPI/FBG sensor with a steel plate was placed on a thermal heater. The temperature increased gradually from 30 $^{\circ}\text{C}$ to 70 $^{\circ}\text{C}$ with a 10 $^{\circ}\text{C}$ increment. Fig. 5 shows the reflection spectrum of the FBG sensor and the relationship between the resonant wavelength and the applied temperature. The Bragg wavelength increases linearly with the increase of temperature. Simultaneously, the cavity length of the EFPI at different temperatures was also measured as presented in Fig. 6. As the temperature increases, the cavity length increases linearly because the increased temperature makes the atoms inside the steel plate and magnets vibrate intensively. The vibration of the atoms leads to the disordered pattern and thus decreases the magnetic force between steel plate and magnet. Fig. 5(b) and 6 can be used to compensate the thermal effect on the cavity length change of the EFPI in actual applications.

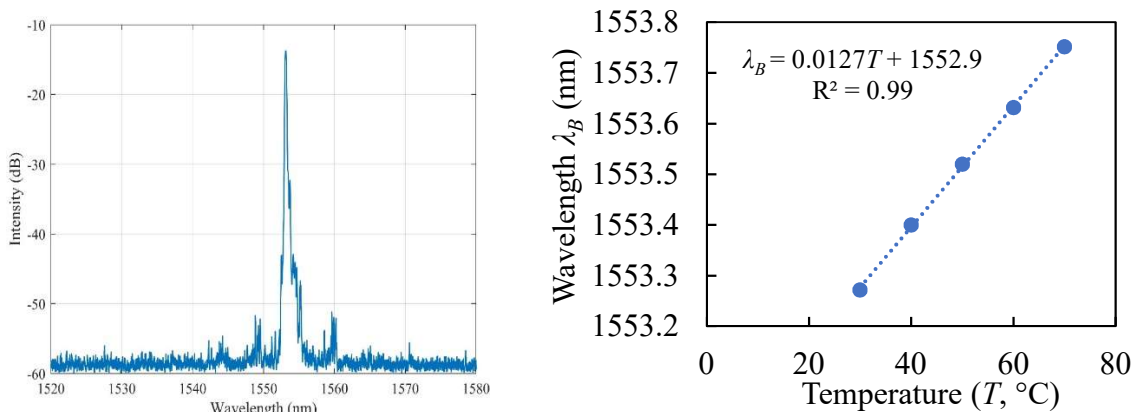


Fig. 5. Measurement from the FBG: (a) reflectance spectrum, and (b) relationship between the resonant wavelength and temperature.

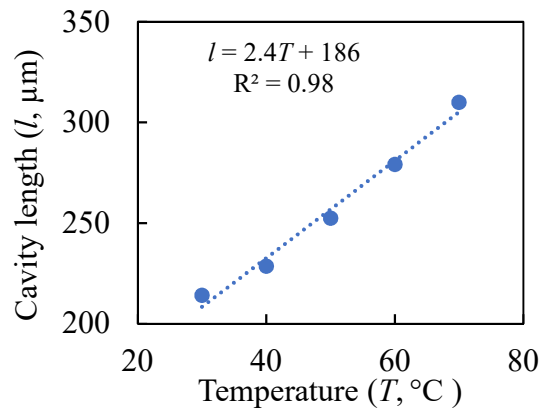


Fig. 6. Change of the cavity length with the testing temperature.

Cathodic protection is widely used along with epoxy coatings to protect a pipeline from corrosion. The cathodic potential applied on a pipe depends upon the size of the pipeline and the outside coating quality. However, electromagnetic interference due to the cathodic protection may distort the magnetic field between the permanent magnet and the steel pipe in the EFPI component of a hybrid sensor. In this study, the steel plate was subjected to a gradually increasing DC voltage from 0 to 30 V. The test results as presented in Fig 7 show that the cavity length remains nearly unchanged as the applied voltage increases. These results confirm that the electromagnetic interference is negligible as found in flowmeter applications.

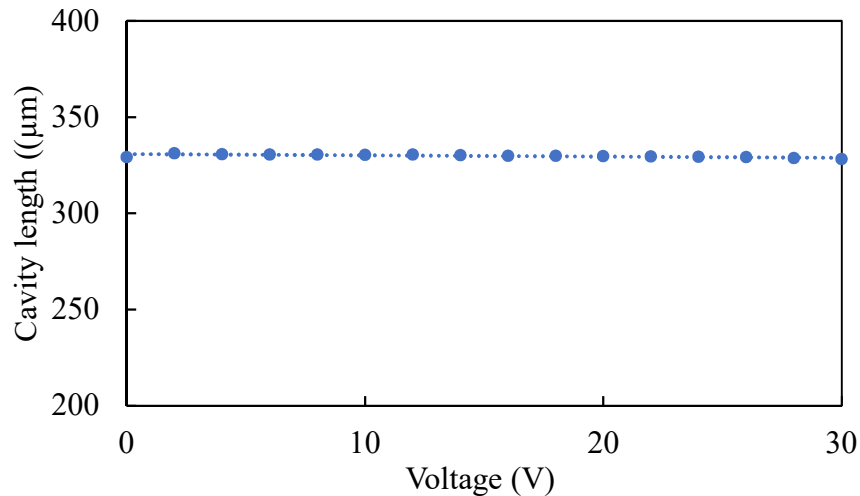


Fig. 7. Test results from a magnet-assisted EFPI: cavity length vs. applied voltage.

Task 2 Development and validation of a graphene-based LPFG sensor with Fe-C coating for improved sensitivity in mass loss measurement in varying temperature environment

To study the temperature effect on the process of corrosion monitoring, a temperature of 20, 40 or 60 °C was applied on the Fe-C coated LPFG sensor through the temperature-controlled water bath. As shown in Fig. 8, the Fe-C coated LPFG corrosion sensor was fixed on the glass slide using marine epoxy. The fiber loop was connected to a high-speed interrogator (Micron Optics Si255) for transmission spectra acquisition. The Fe-C layer was connected to a potentiostat (model: Gamry Interface 1000E) through a copper wire using silver conductive epoxy (MG Chemicals 8331) as the working electrode during electronic impedance spectroscopy (EIS) tests. Open circuit potential (OCP) was measured before the EIS. The EIS was conducted at 5 points per decade with the frequency range from 5 mHz to 100 kHz and a sinusoidal potential of 10 mV around OCP.

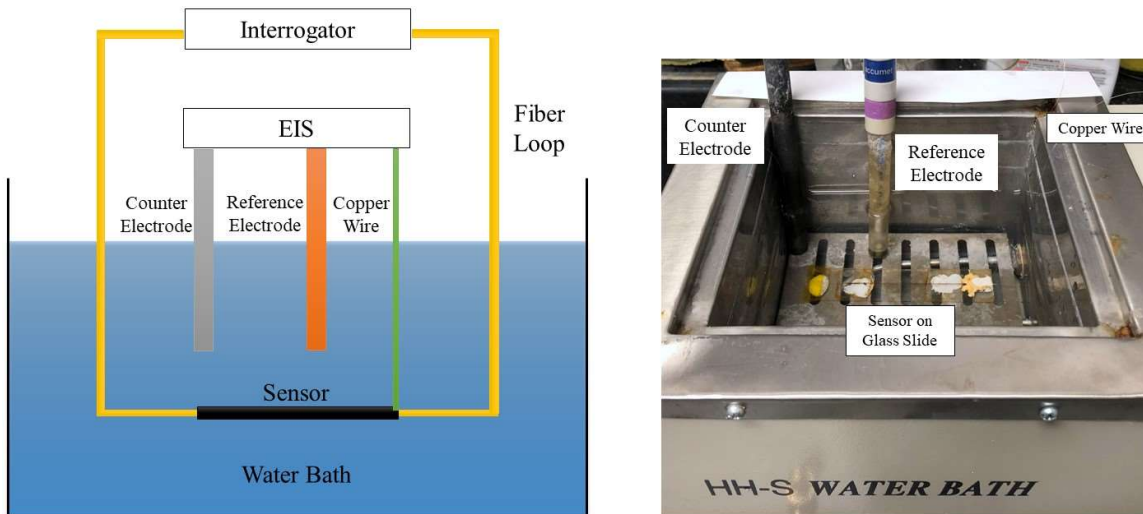


Fig. 8. Schematic view and laboratory setup of the corrosion test under various temperature levels.

The correlation between the mass loss of the Fe-C layer and the resonance wavelength shift was established using the method proposed and developed in our previous work. As shown in Fig. 9, the three stages, sensor sensitivity and transition mass loss between Stage I and II are considered to be the same for the three temperature conditions, indicating that the sensor has a robust performance for pipeline corrosion monitoring under 60 ° C.

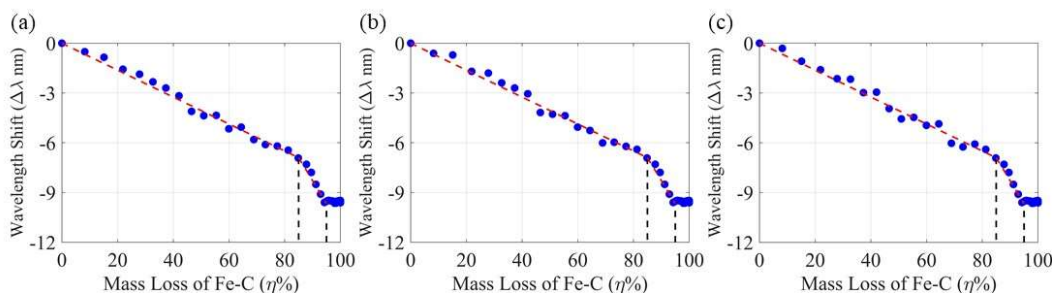


Fig. 9 Correlation between mass loss and resonance wavelength shift under three temperature levels.

To characterize the attenuation of evanescent field in radial direction of optic fibers, three long period fiber gratings (LPFG) sensors coated with a varying number of graphene (Gr) layers were prepared and tested. Monolayer Gr was first synthesized on the top side of a copper (Cu) foil through a low pressure chemical vapor deposition (LPCVD) system. The Gr/Cu sample was then coated by a thin uniform layer of Poly(methyl methacrylate) (PMMA, $M_w=996,000$, Sigma Aldrich) as a “tape” to make graphene fragments stick together. Next, the sample was floated on the copper etchant solution for 4 hours to dissolve the copper foil and obtain a PMMA/Gr transparent film. The PMMA/Gr transparent film, while floating in the solution, was supported underside by another graphene layer on a copper foil. The copper foil was lifted gradually to ensure that the new graphene was fully covered by the film. The dissolution process of copper and the transfer operation of graphene were repeated alternatively until three layers of graphene were stacked together. Next, the three-layer graphene was transferred onto a LPFG sensor, which was fixed on a glass slide. Multiple LPFG sensors coated with the same number of graphene layers can be prepared at the same time to increase work efficiency, as shown in Fig. 10. Finally, the PMMA layer outside the graphene layers was removed in an acetone bath to obtain the Gr-coated LPFG. The above process can be repeated to coat a three-layer graphene on the LPFG sensor each time. Transmission spectra of LPFG sensors coated with a different number of graphene layers were recorded using an optical interrogator (Micron Optics Si255). Transmission spectra of a representative LPFG sensor (no. 2 as designated later) was presented in Fig. 11.

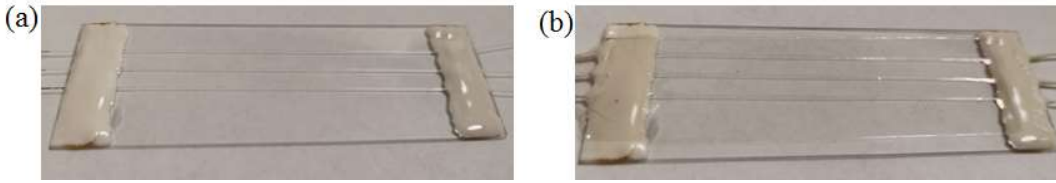


Fig. 10. Three LPFG sensors: (a) without graphene coating, (b) with graphene coating.

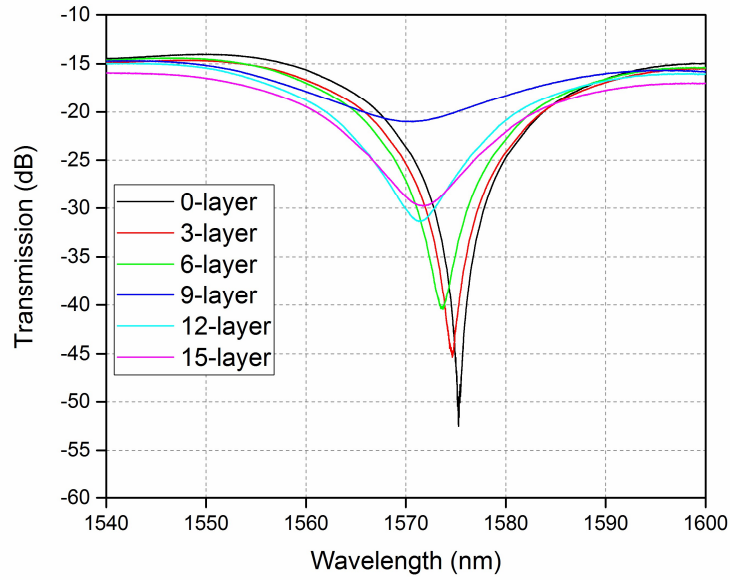


Fig. 11. Transmission spectra of a LPFG sensor coated with a varying number of graphene layers.

At the beginning of sensor preparation, one LPFG sensor was broken accidentally. Thus, the test results of two LPFG sensors were reported herein. The resonant wavelengths of the two LPFG sensors coated with different numbers of graphene layers were summarized in Table 1, and the wavelength shifts were presented in Fig. 12.

Table 1 Resonant wavelengths (nm) of two LPFG sensors coated with different numbers of graphene layers

Number of graphene layers	Wavelength (nm)	
	Sensor 1	Sensor 2
0	1574.9	1575.3
3	1570.4	1574.6
6	1569.5	1573.7
9	1564.3	1570.6
12	1560.9	1571.3
15	1560.9	1571.7

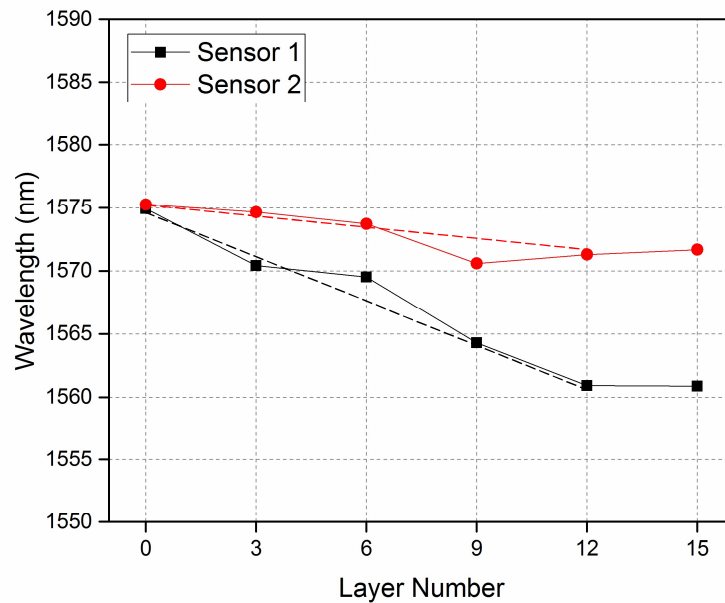


Fig. 12. Wavelength shift of two LPFG sensors with a different number of graphene layers.

Fig. 12 also shows two linear trending lines (no regression analysis) between the wavelength shift of a LPFG sensor and the number of graphene layers. Overall, it can be observed from Fig. 12 that the wavelength of LPFG sensors decreased linearly with the increase in number of graphene layers. The sensitivities of the two sensors were quite different though their initial wavelengths were nearly the same. This comparison indicated a more significant bending effect in Sensor 2 for reduced sensitivity in the process of repeated graphene applications.

The wavelength shift appeared to stop when the number of graphene layers reached 12. This result indicated an evanescent field depth of approximately 4 nm. The wavelength shift of Sensor 1 corresponding to six layers of graphene seemed an outlier. The wavelength shift of Sensor 2 corresponding to nine layers of graphene seemed an outlier. As indicated by the irregular and flatten transmission spectrum shown in Fig. 11, the last added three graphene layers in Sensor 2 had a significant number of wrinkles that cause a sudden reduction of transparency and thus reduce the loss of light energy in the form of evanescence field in addition to the global bending effect. The exact reasons of these outliers in Sensors 1 and 2 are yet to be studied in the future.

Three additional LPFG sensors were prepared and tested to characterize the attenuation of evanescent field in radial direction of the optic fiber by coating a varying number of graphene (Gr) layers. Though this method could increase work efficiency, it also presented some challenges. After graphene is coated on LPFG sensors, heating is necessary to make graphene and sensors fit tightly, but heating causes the inelastic deformation of an optical fiber. Although the inelastic deformation caused by one heating operation is very small, as the number of layers of coated graphene increases, the number of heating times will also increase, resulting in the accumulation of inelastic deformation on the optical fiber to an obvious extent, as shown in Fig. 13. Since the two ends of the optical fiber are fixed, the accumulated inelastic deformation will make the optical fiber in a bending state, which will interfere with the measurement results. To solve this problem, a new experimental design was proposed.

The new experimental design used a two-layer glass slide that has one movable end, as shown in Figs. 14 and 15. In Fig. 14, the numbers in yellow circles represent three different glass slides. The two ends of the LPFG sensor are fixed on slides 1 and 2, respectively. Slide 1 is fixed on the top of slide 3 by marine epoxy to ensure no relative movement. Slide 2 is allowed to move on the top surface of slide 3, which makes it possible and convenient to adjust the distance between two ends of the LPFG sensor.

Slide 2 could be fixed on slide 3 by yellow high temperature resistant tapes when needed, as shown in Fig. 15. Stripping off the tapes would allow slide 2 to move to accommodate potential heat-induced deformation in order to keep the LPFG sensor straight over time. The transmission spectra of a LPFG sensor in curved and straight states are compared in Fig. 16. It is obvious that the curvature of the optic fiber affects the resonant wavelength and attenuation of the signal.



Fig. 13. Three LPFG sensors using the previous design.

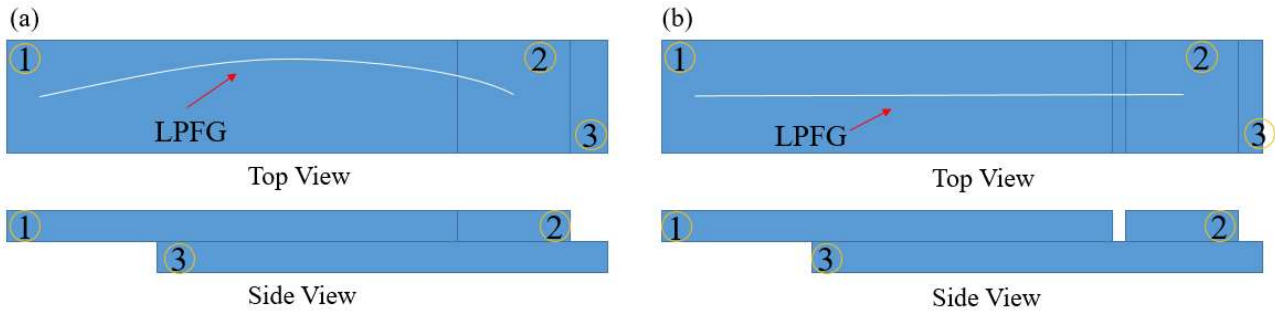


Fig. 14. Schematic illustration of the new test design: (a) curved LPFG, and (b) straight LPFG.

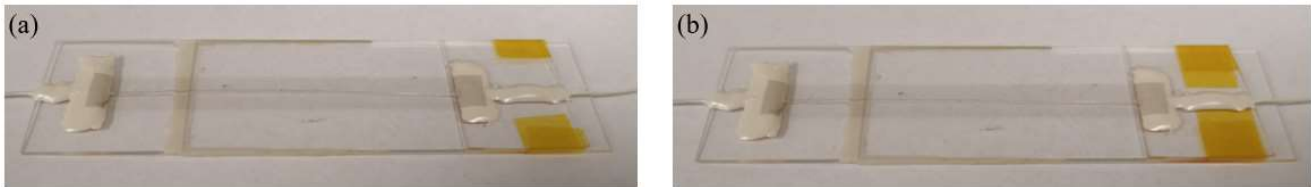


Fig. 15. Real photos of the new test design: (a) curved LPFG, and (b) straight LPFG.

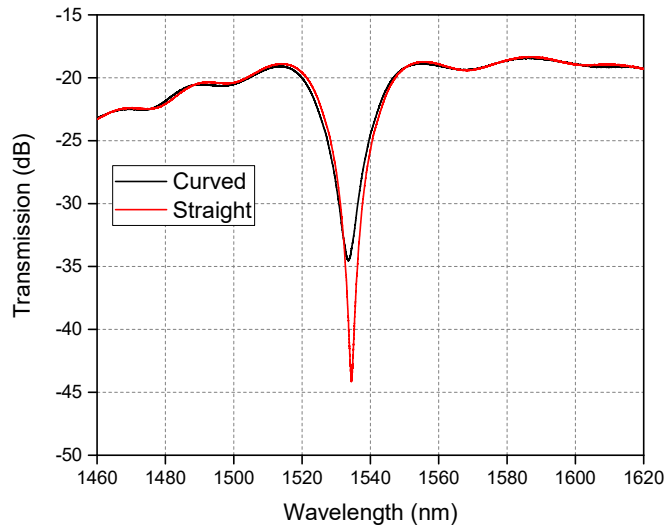


Fig. 16. Transmission spectra of a LPFG sensor in curved and straight states.

Two out of the three LPFG sensors were broken at the beginning of the coating process accidentally. Thus, only the test results of the third LPFG sensor were reported herein. Transmission spectra of the intact LPFG sensor (no. 4 as designated later) was presented in Fig. 17(a). The resonant wavelengths of the LPFG sensor (no.4) coated with a varying number of graphene layers were summarized in Table 2, and

the wavelength shifts were presented in Fig. 17(b).

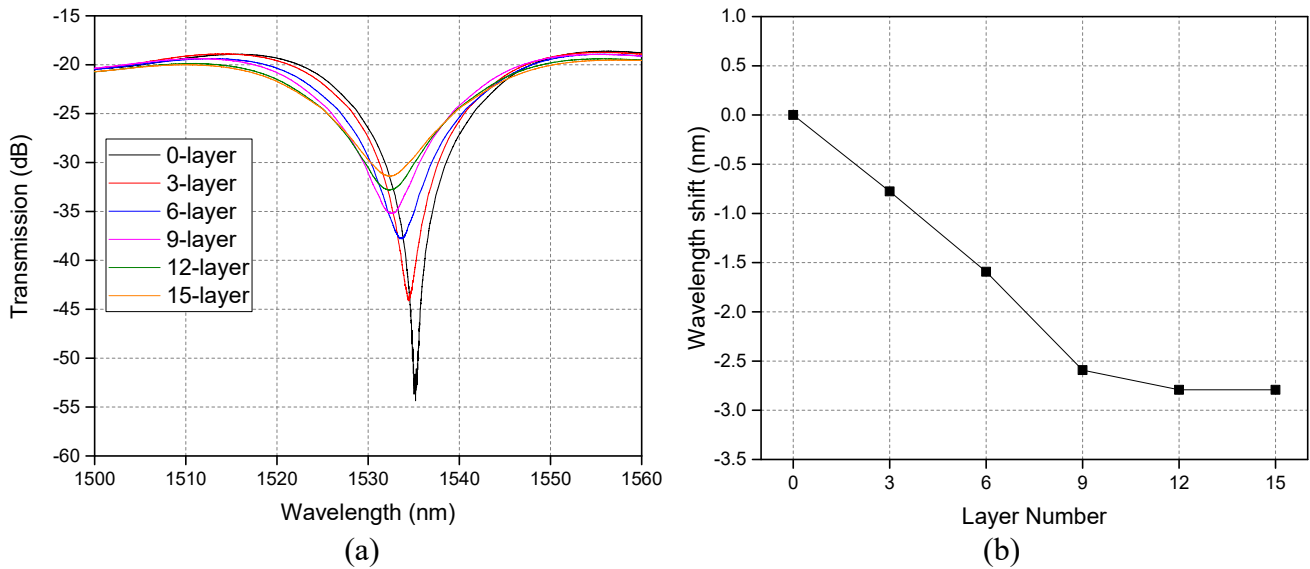


Fig. 17. Measurement from the LPFG sensor (no.4) coated with a varying number of graphene layers: (a) transmission spectra, and (b) wavelength shift.

It can be observed from Fig. 17(b) that the wavelength of LPFG sensors decreased linearly with the increase in number of graphene layers. The wavelength shift appeared to stop when the number of graphene layers reached 12. This result indicated an evanescent field depth of approximately 4 nm since the thickness of 3-layer graphene is about 1 nm. This conclusion is consistent with the previous results of the last quarter.

Table 2 Resonant wavelength shift of LPFG sensor (no.4) coated with different numbers of graphene layers

Number of Gr layers	Wavelength Shift (nm)
0	0.0
3	-0.8
6	-1.6
9	-2.6
12	-2.8
15	-2.8

Task 3 Integration and field validation of multiple FBG/EFPI and multiplexed LPFG sensors for internal and external corrosion monitoring of a pipeline with temperature compensation.

To integrate a FBG/EFPI sensor into a sensor package in field applications, two designs of the sensor were proposed. One design is spring-based, and the other design is plate-based, as shown in Fig. 18(a) and 18(b), respectively. The spring-based design was abandoned since it was difficult to keep the magnet horizontal and bond springs to other components closely. For the plate-based design, the fiber has to be fixed on the acrylic plate vertically, which requires an extra component to hold it. In addition, once the fiber is stuck to the vertical component, its angle of inclination can no longer be adjustable. The signal quality highly depends on the angle between the fiber and the mirror. The closer the angle is to 90°, the

better the signal quality. To reduce the difficulty of sensor fabrication, a new improved design was proposed as shown in Fig. 19.

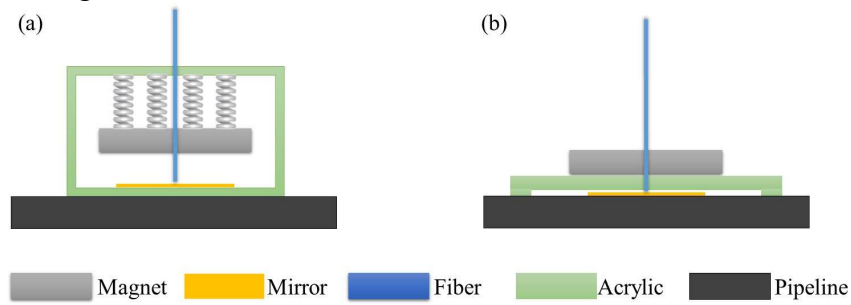


Fig. 18. Schematic illustration of two sensor package designs: (a) spring-based, and (b) plate-based.

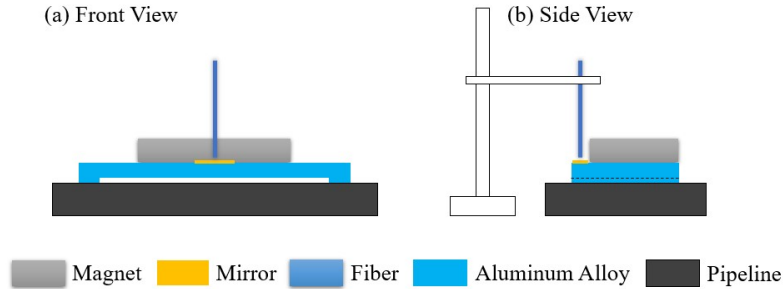


Fig. 19. Schematic illustration of the improved plate-based sensor package design.

The new design is based on the plate-based sensor as proposed before. However, a magnet is placed on top of an aluminum alloy plate instead of an acrylic plate since aluminum alloy has a higher elasticity modulus and thus could decrease the thickness of the plate, which increases the sensitivity of the sensor. In addition, a mirror is placed on top of the aluminum alloy plate while the fiber is fixed by a holder outside the sensor. The holder could adjust the height and the inclination angle of the fiber to increase the signal quality.

Fig. 20 shows the prototype of the new sensor design for laboratory validations and calibrations. Similar to the previous tests reported, a steel plate with an EFPI sensor deployed above was connected to the positive electrode in the DC circuit. Accelerated corrosion current was applied during the test and the EFPI interference pattern was recorded from an optical interrogator (Micron Optics Si 255). The cavity length between the fiber and a gold coated mirror was recorded to explore the relationship between the cavity length shift and the mass loss of the steel plate.

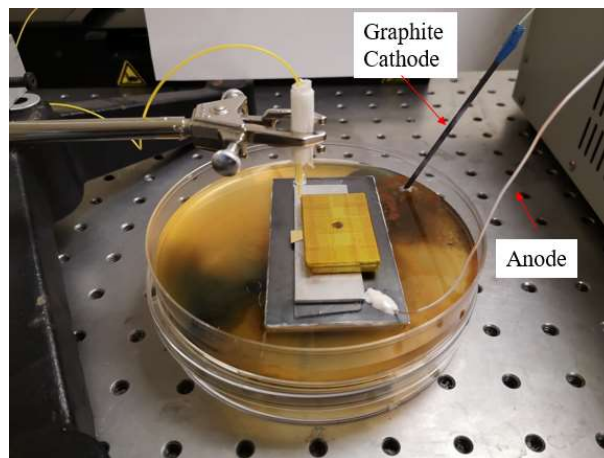


Fig. 20. Prototype of the improved plate-based sensor for laboratory tests.

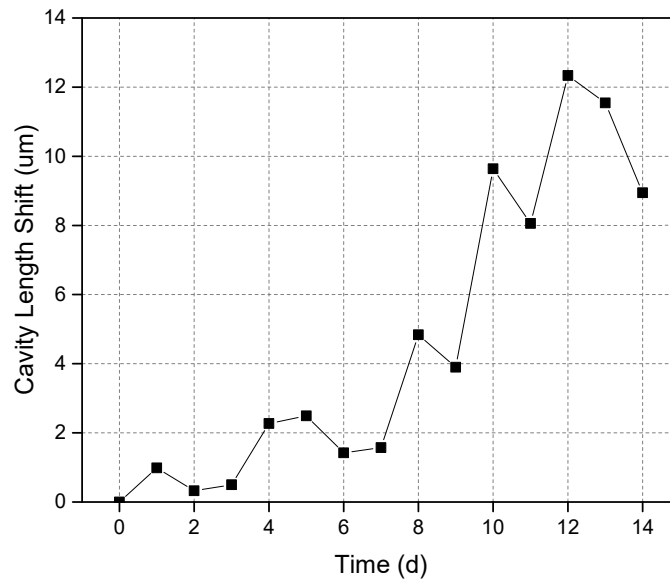


Fig. 21. Cavity length shift over time in the creep and corrosion test.

Fig. 21 shows the cavity length shift over time in the creep and corrosion test. The data in the first 7 days are for creep test, and the data in the last 7 days are for corrosion test. As the corrosion process continues, the magnetic force between the magnet and the steel plate expects to decrease and the aluminum plate expects to deform to a less degree. As a result, the cavity length of the EFPI sensor expects to decrease. However, the experimentally determined cavity length generally increases with time, which is counter intuitive. This problem is likely caused by the creep effect of the aluminum alloy plate. The creep effect increases the deflection of the aluminum plate, reduces the distance between the magnet and the steel plate, and thus increases the magnetic force. The increase of the magnetic force in turn increases the creep effect. The increase in wavelength by the creep effect is more than the decrease by the corrosion effect. As a result, the test results show an increase of the cavity length shift instead of reduction. This explanation warrant further verification in the following study.

(c) Planned Activities for the Next Quarter - The following activities in Task 2 and Task 3 will be executed during the next reporting quarter.

Task 2 Development and validation of a graphene-based LPFG sensor with Fe-C coating for improved sensitivity in mass loss measurement in varying temperature environment

The evanescent field attenuation will continue to be characterized.

Task 3 Integration and field validation of multiple FBG/EFPI and multiplexed LPFG sensors for internal and external corrosion monitoring of a pipeline with temperature compensation.

The creep effect will be researched to get meaningful results.

(d) Problems Encountered during this Quarter and Potential Impact on Next Quarter – This project continues to be impacted by COVID-19. To keep six feet apart between any two students in laboratory, limited laboratory access is available to students. As such, students sometimes have to work in shift.